Aerodynamic Prediction and Performance Analysis for Mars Science Laboratory Entry Vehicle

Tang Wei, Yang Xiaofeng, Gui Yewei, Du Yanxia

Abstract—Complex lifting entry was selected for precise landing performance during the Mars Science Laboratory entry. This study aims to develop the three-dimensional numerical method for precise computation and the surface panel method for rapid engineering prediction. Detailed flow field analysis for Mars exploration mission was performed by carrying on a series of fully three-dimensional Navier-Stokes computations. The static aerodynamic performance was then discussed, including the surface pressure, lift and drag coefficient, lift-to-drag ratio with the numerical and engineering method. Computation results shown that the shock layer is thin because of lower effective specific heat ratio, and that calculated results from both methods agree well with each other, and is consistent with the reference data. Aerodynamic performance analysis shows that CG location determines trim characteristics and pitch stability, and certain radially and axially shift of the CG location can alter the capsule lifting entry performance, which is of vital significance for the aerodynamic configuration design and inner instrument layout of the Mars entry capsule.

Keywords—Mars entry capsule, static aerodynamics, computational fluid dynamics, hypersonic.

I. INTRODUCTION

MOTIVATED by the curiosity about the universe origin, the search for the extraterrestrial intelligence, and the interest in the space recourses exploitation, exploration missions to Mars have been carried out several times since 1960s. Mars landing probe is surrounded with non-air gas during its entry into the Martian atmosphere. Hypersonic flow exists around the probe, and as a result severe aerodynamic force and aero-heating occur on the probe surface. Therefore, specific aerodynamic and thermal protection problems are brought forth. Mars entry missions have some similarity to Earth reentry missions, but remarkable difference exists at the same time.

The recent Mars entry mission is called Mars Science Laboratory (MSL), which successfully landed on the Mars surface on August 2012.The MSL entry capsule traveled the entire Martian atmosphere before descending and landing [1], [2], and selected complex lifting entry for sufficient deceleration and precise landing performance. The hypersonic lift-to-drag (L/D) is designed for 0.24 at the trimmed angle of attack of 16°.The capsule center of gravity (CG) is radially

Tang Wei, Yang Xiaofeng, and Du Yanxia are with the State Key Laboratory of Aerodynamics, China Aerodynamics Research and Development Center, Mianyang Sichuan 621000,China (e-mail: Tangwei@cardc.cn, yangxiaofeng@cardc.cn, yanxiadu@cardc.cn).

Gui Yewei is with the State Key Laboratory of Aerodynamics, China Aerodynamics Research and Development Center, Mianyang Sichuan 621000,China (corresponding author, e-mail: guiyewei777@126.com).

offset to meet the demand of the trimmed angle of attack and L/D [3]. Such entry technique was also adopted by most of the Earth reentry capsules, such as Soyuz. How to precisely predict the lifting entry process is one of the most important problems for Mars entry capsule design.

Though several Mars entry missions have been achieved, small amount of flight data is available. In addition, there exist no ground-based facilities that can reproduce the high-speed and high-temperature flow close to the Martian environment. The computational fluid dynamics technique, therefore, turns out to be a significant approach for flight aerodynamic analysis. For hypersonic Mars entry, Navier-Stokes equations solver is believed to be applicable for flowfield prediction and aerodynamic performance analysis, because the peak surface pressure occurs in the continuum regime.

Up to now, lots of numerical works for hypersonic flow have been made to evaluate the aerodynamics for different configurations. Most of the numerical works used the complicated chemical and thermal non-equilibrium model, which have not been effectively verified by experiments [4]. Therefore, some computational attempts based on the perfect gas model have been made to avoid the uncertainty of the chemical reacting model, and comparative discussions with the complex reacting model were also performed [5]-[8]. For the Mars entry process, because the atmosphere differs from the air, the real post-shock effective specific heat ratio γ_2 is less than that of reentry process [5]. Therefore, the specific heat ratio is no longer assumed to be 1.4 for Mars entry process, and aerodynamic coefficients may thus alter in the Mars entry case. The specific heat ratio is mainly the function of temperature, as is demonstrated in statistical thermodynamics [9]. We can use the effective specific heat ratio to simulate the hypersonic non-air flow with high temperature real-gas effects [10]. Such approach has been widely used in the rocket combustion flow, hypersonic reentry flow [11], [12] and so on.

In this paper, we developed the three-dimensional numerical method for precise computation and the surface panel method for rapid engineering prediction. A serial of numerical and engineering simulations for the MSL entry capsule were performed at different angle of attack at a given flight state based on the specified effective specific heat ratio assumption. Detailed flowfield analysis and the static aerodynamic performance were then discussed to provide the aerodynamic design suggestions.

II. METHODS

A. Numerical Simulation Methods

Computational Fluid Dynamics technique was undertaken to

predict the aerodynamic force for the Mars entry vehicle. A finite volume approach was used to solve the full Navier–Stokes flowfield equations for a calorically perfect gas. The code used the van Leer flux-vector splitting method for the inviscid fluxes with the 2nd order correction using the van Leer limiter. For time integration, the non-iterative implicit method was used for rapid convergence.

Constant inflow condition was imposed on the far field boundary, and the extrapolation was used on the outflow boundary in all solutions. Non-slip wall boundary condition was implemented and the thermal state of the surface is radiative equilibrium with a fixed surface emissivity of 0.78.

The flowfield is assumed to be steady and laminar. Unsteady effects are weak at these high speeds for long duration entry flight [13], and moreover, unsteady aerodynamic contribution is negligibly small in the afterbody [14]. Transition to turbulence could occur but is weak due to low Reynolds number in the relatively thin Martian atmosphere [4].

High-temperature gas viscosity coefficient is assumed to depend only on temperature, and can be specified by Sutherland's law [15]. The dynamic viscosity coefficient μ for Martian gas is:

$$\frac{\mu}{\mu_0} = \left(\frac{T}{T_0}\right)^{\frac{3}{2}}(T_0 + C)/(T + C) \tag{1}$$

where the reference viscosity $\mu_0 = 1.48 \times 10^{-5}$ kg/(m·s), the reference temperature $T_0 = 293.15$ K, and the Sutherland constant $C = 240$ K. Sutherland's law agrees well with theoretical calculation from Fenghour [16].

For high-temperature Martian gas, we assume $Pr = 0.71$, which is used to obtain the thermal conductivity $k=\mu c_p/Pr$.

B. Engineering Prediction Method

Surface panel method was used to calculate the surface pressure coefficient for rapid prediction. The pressure coefficient for each individual element is the function of inflow velocity vector, the element area and the surface normal vector of the given element, and has no relation with the neighbor element. The total aerodynamic coefficients are then calculated by integrating the panel pressure coefficient along the total surface.

The main work of the surface panel method is to calculate the surface pressure coefficient. Multiple engineering methods to predict the surface pressure coefficient have been developed so far, with their peculiar applications. The modified Newtonian theory is believed to be quite suitable for hypersonic aerodynamics prediction of blunt body, such as reentry shapes, Mars entry capsules, etc. The modified Newtonian formula can be described as:

$$C_p = C_{pmax}(\bar{V}_\perp/V_\infty)^2 \tag{2}$$

where C_{pmax} is the stagnation pressure coefficient, described as:

$$C_{pmax} = \frac{2}{\gamma Ma_\infty^2}\left[\left(\frac{(\gamma+1)^2 Ma_\infty^2}{4\gamma Ma_\infty^2 - 2(\gamma-1)}\right)^{\frac{\gamma}{\gamma-1}} \cdot \left(\frac{1-\gamma+2\gamma Ma_\infty^2}{\gamma+1}\right) - 1\right] \tag{3}$$

It can be seen that the stagnation pressure coefficient is the only function of inflow Mach number and the specific heat ratio.

It is noted that the modified Newtonian formula is valid for windward region, and the coefficient in the leeward region is assumed to be zero because the pressure effect here is negligibly weak. The velocity ratio is the cosine of the angle between the inflow velocity and the surface normal vector.

C. Effective Specific Heat Ratio Method

Multicomponent mixture exists in the Martian atmosphere, including approximately 95% CO2, 3% N2, 2% Ar and other negligible species. Since the real values of specific heat ratio markedly decrease at high-Mach-number flight conditions when the gas goes across the shock, effective specific heat ratio was specified to take the non-air and high-temperature real-gas effects into account. The post-shock specific heat ratio, which only depends on the local temperature for thermal perfect gas, is expected to be the effective value γeff. Considering the vibrational excitation, the local specific heat ratio is:

$$\gamma = \sum_{j=1}^{m} w_j c_{P,j} / \sum_{j=1}^{m} w_j c_{V,j} \tag{4}$$

where m is the number of gas species, w_j is the mass fraction of the species j. For each species, c_p and c_v are determined by molecular transitional, rotational and vibrational energy, so we have

$$c_V = \left(\frac{1}{2}n_t + \frac{1}{2}n_r + \sum_{i=1}^{n_v} \frac{\left(\frac{T_{v,i}}{T}\right)^2 e^{\frac{T_{v,i}}{T}}}{\left(e^{\frac{T_{v,i}}{T}} - 1\right)^2}\right) R \tag{5}$$

$$c_P = c_V + R$$

where n_t, n_r and n_v, are the molecular transitional, rotational and vibrational degrees of freedom, and $T_{v,i}= hv_i/k$ is the vibrational characteristic temperature, determined by the vibrational characteristic frequency v_i referred by [**].

The local post-shock temperature can be simply obtained by solving the generalized Rankine-Hugoniots hock relation. For normal shock, we have:

$$\left(\frac{\rho_2}{\rho_\infty}\right)^2\left[M_\infty^2 + \frac{2}{\gamma_\infty - 1}\right] + \left(\frac{\rho_2}{\rho_\infty}\right)\left[-\frac{2\gamma_2(\gamma_\infty M_\infty^2 + 1)}{\gamma_\infty(\gamma_2 - 1)}\right] + \left[M_\infty^2 \frac{\gamma_2 + 1}{\gamma_2 - 1}\right] = 0 \tag{6}$$

$$\frac{\frac{p_2}{p_\infty} - 1}{\gamma_\infty M_\infty^2} = \frac{\frac{p_2}{p_\infty} - 1}{\frac{p_2}{p_\infty}} \tag{7}$$

$$\frac{T_2}{T_\infty} = \frac{p_2}{p_\infty}\frac{\rho_\infty}{\rho_2}\frac{R_\infty}{R_2} \tag{8}$$

By iterating formulae (4) to (8), we obtain the local specific heat ratio γ_2 in the shock layer, which is considered to be the effective specific heat ratio γ_{eff}. It must be noted that the effective value is valid only in the stagnation region, but we can generalize it to the overall flowfield because the stagnation aeroforce is dominant and such difference is negligibly small. The effective specific heat ratio contours with the inflow Mach number and temperature are shown in Fig. 1. In the infinite case

($M\infty \to \infty$), γ_{eff} tends to a specific value because of full excitation of vibrational energy and the stagnation pressure coefficient gets independent on the inflow Mach number.
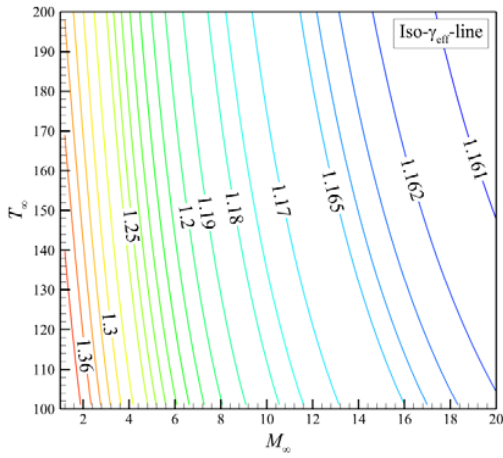

Fig. 1 Effective specific heat ratio contours with inflow Mach number and temperature

D. Validation Case

The validation model is a scaled 70° sphere-cone configuration with the available numerical and experimental data from [17], [18]. The wind tunnel experiment use CO_2 as the test gas with the inflow enthalpy of 1.89MJ/kg ($U_\infty = 1908$ m/s, $p_\infty = 1010$ Pa). Calculated results from numerical simulation and engineering prediction based on the effective specific heat ratio method are compared against the experimental data. The calculation results of the surface pressure from both two mentioned approaches, the DPLR data and the experimental data are all shown in Fig. 2 for comparison. The comparison highlights a good agreement between calculated and experimental data, thus confirming reliability of the numerical simulations and engineering prediction for Mars entry capsules.
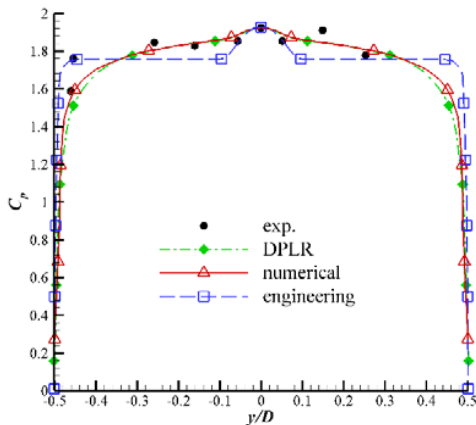

Fig. 2 Surface pressure comparison with experimental data and DPLR data for the inflow enthalpy of 1.89 MJ/kg

III. Results and Discussion

A. Geometry and Grid Generation

The proposed geometry for aerodynamic performance analysis is the Mars Science Laboratory entry vehicle with a 70-degree sphere-cone forebody and three-sectional-cone afterbody as described in Fig. 3. The body axis system is used for aerodynamic performance analysis also shown in Fig. 3, in which system a pitch-up motion means a positive angle of attack ($\alpha > 0$), and a positive pitch moment pitches the capsule up.
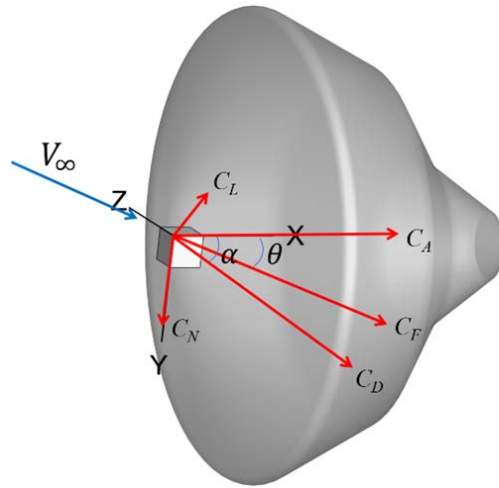

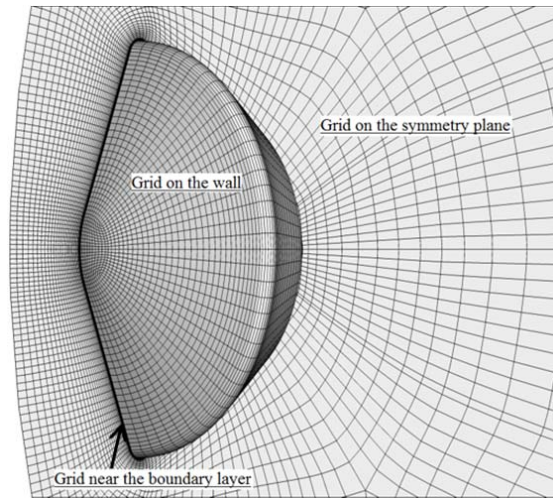Fig. 3 MSL geometry and definition of aerodynamic forces

Fig. 4 MSL computational grid schematic (the actual grid is twofold refined in each direction)

Two-dimensional surface grid is required for rapid aerodynamic prediction using the panel method, while full three-dimensional grid is necessary for numerical simulation of overall flowfield. The computational grid for MSL configuration is a multi-block structured grid, mainly growing from the surface grid taking the boundary layer into consideration, and has an overall number of approximately 1.4

million cells for half body. To assure accurate prediction, the grid is everywhere orthogonal to the body at the surface. Grid independence analysis shows that grids for the wall cell Reynolds number $Re_c=\rho_\infty U_\infty d_w/\mu_\infty$ can fulfill the accuracy requirement of aerodynamics analysis, where d_w is the normal grid distance close to the wall (the wall step). The wall cell Reynolds number for the current analysis is hence 6.4. Fig. 4 shows both the two-dimensional surface grid and the grid on the symmetry plane.

B. Mars Entry Flowfield

In order to figure out the detailed hypersonic flowfield, steady numerical simulations for a specific hypersonic flight state are herein performed. The flight speed is 5164 m/s and the Mach number is 26.1 with an angle of attack $\alpha = -17.05°$, so that the inflow unit Reynolds number $Re_\infty=2.4\times10^6$/m. The effective value of specific heat ratio used in the calorically perfect gas flow simulation is derived to be 1.16.
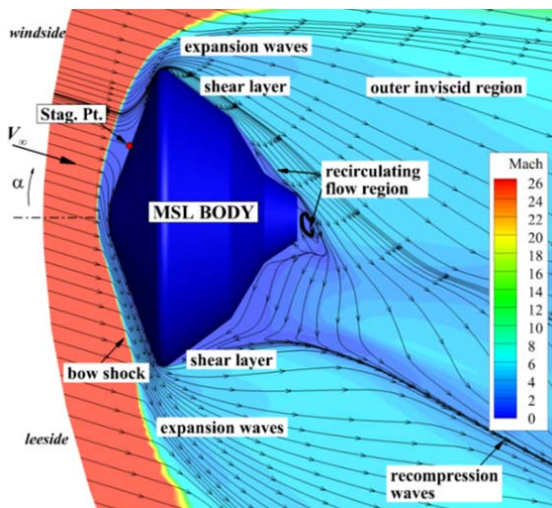

Fig. 5 Hypersonic flow structure for MSL on the symmetry plane

Hypersonic flowfield for the MSL entry vehicle is complicated, especially for the vortex flow. Fig.5 shows the main steady structure of the hypersonic flow on the symmetry plane. A strong bow shock wave is detached from the surface and lies very close to the heat shield. The gas across the shock wave is compressed to form a shock layer, much thinner than that of the air flow. Inflow uniform streamlines are deflected across the shock and travel around the body (Fig. 6). Expansion waves occur near the shoulder due to large deflection angle. The gas gets accelerated in this region and merges into the external inviscid flow downstream from the shoulder. The heat shield boundary layer thickness increases from the stagnation point to the shoulder, and the shear layer appears after the shoulder, resulting in local vortex motion. Consequently, flow separation arises on the backshell (Fig. 6). A large region of recirculating flow leads to relatively low pressure distribution on the backshell, which has a negligible contribution to the total coefficients. The wake flow after the capsule meets and then accumulates to form the recompression waves, which are

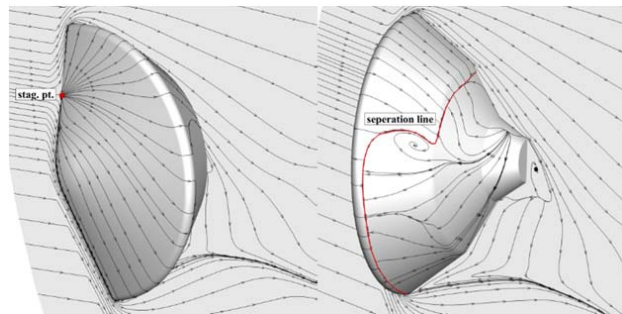nearly parallel to the inflow direction, and grow weaker to the outer flow.

Fig. 6 Streamlines on the symmetry plane and near the surface of MSL

C. Surface Pressure Distribution

For the same inflow boundary condition, rapid engineering calculation was performed to obtain the surface pressure and the total aerodynamic coefficients. The calculated surface pressure coefficient distribution is shown in Fig. 7. Compared with the numerical results, the rapid prediction results regularly spread on the cone frustum from the heat shield apex, due to the single dependency of pressure coefficient on geometry angle.

Fig. 8 shows the heatshield surface pressure coefficient distribution on the symmetric line, including the numerical results, engineering prediction values and the reference data [3] for comparison. As is expected, the surface pressure is the highest at the stagnation point and falls off rapidly as the flow expands around the shoulder and onto the afterbody. On the whole, calculated results for surface pressure from numerical simulation and engineering calculation keep in good agreement with the reference, especially on the windward region, which dominates the total aeroforce coefficients.

It is noted that a certain degree of fluctuation exists for numerically calculated surface pressure in the heatshield leeside, partly because of extremely high Mach number and very low specific heat ratio. Nevertheless, the overall influence of such fluctuation is relatively weak after integration for aerodynamic analysis. It maintains the level of surface pressure on the cone frustum because the geometric angle between the wall and inflow velocity holds on the frustum.
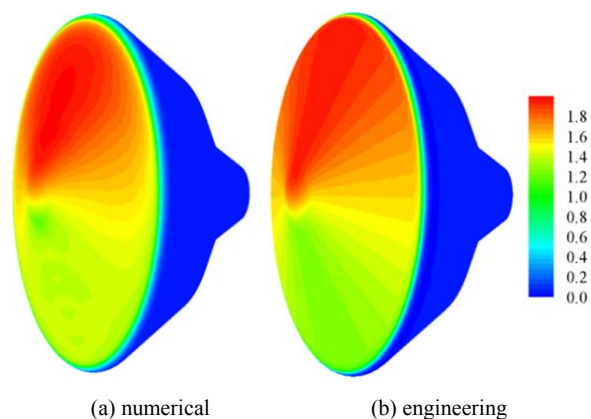

(a) numerical   (b) engineering

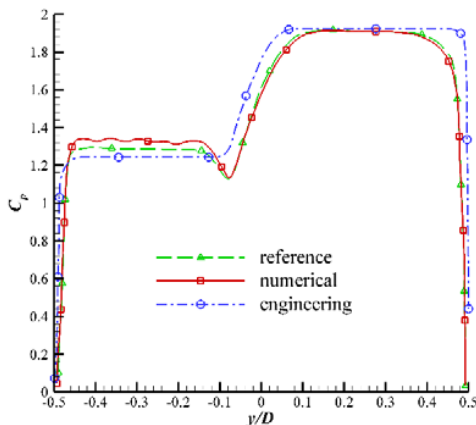Fig. 7 Surface pressure distribution

Fig. 8 Surface pressure distribution on symmetry plane of MSL heat shield

The stagnation point locations, and the shock and sonic lines on the symmetric plane are also shown in Fig. 9. For angle of attack of -6°, the stagnation point is located near the axis on the sphere cone; when the angle of attack increases to -17.5°, the stagnation point is moved far away from the axis to the cone frustum section; when to -29°, the stagnation point is moved very near to the shoulder. The windward sonic line merges into the boundary layer at the shoulder, while the leeward one at different place depending on the angle of attack. For lower angle of attack, -6° for example, the sonic line merges into the boundary layer at the shoulder, the same as the windward one. When the angle of attack increases, the merging location moves to the sphere-cone junction (in -17.5° case), even near the axis (in -29° case), and the sonic line has an inflection in the vicinity of the apex because of strong compressibility. The high pressure region is surrounded by the windward sonic line and the wall, which dominates the total aerodynamic coefficients, particularly at small angles of attack.
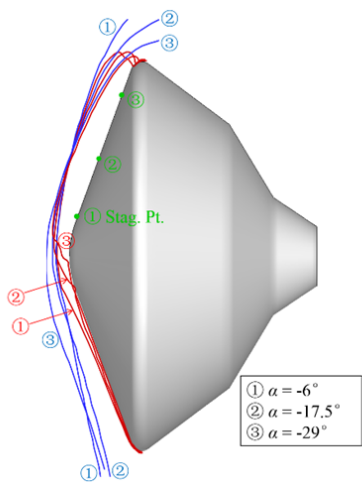

Fig. 9 Shock wave and sonic line for different angle of attack

D. Aerodynamic Coefficients

The integrated lift (C_L) and drag (C_D) coefficients and the lift-to-drag ratio (L/D), are shown in Fig. 10 as a function of angle of attack from zero to -45° for both numerical and engineering results. Both results keep the same trend as to the angle of attack, and the values of them are quite close in low angle of attack. At large angle of attack, the windward flow differs remarkably from the leeward flow, which cannot be captured by surface panel method, so that the total coefficients have much different. C_D is predicted to decrease continuously as the magnitude of the angle of attack increases and C_L is just the reverse in the relatively low angle of attack. As a result, L/D increases with the increase of the magnitude of the angle of attack. It can be expected from computations that a trimmed L/D of 0.27 can be achieved if a trimmed angle of attack of 17.5°holds. Moreover, C_D is expected to be dominant in all total coefficients, which is the typical character of blunt entry capsule.
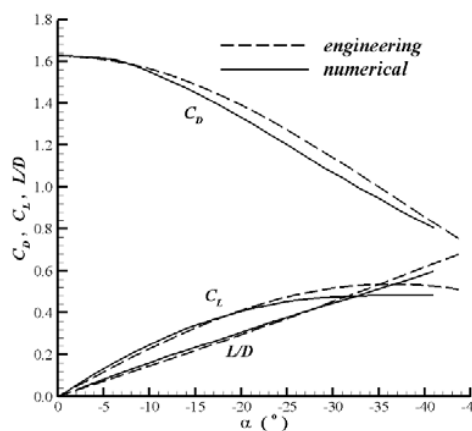

Fig. 10 The total coefficient curves for both numerical and engineering results

E. Center of Gravity and Stability Analysis

For hypersonic lifting entry process, there exists a close relationship between the center of gravity (CG) location and the flight performance with can be described by:

$$X_{cg} = X_{cp} - \Delta X , \ Y_{cg} = Y_{cp} - \Delta Y \ ,$$

$$\Delta X = \frac{\frac{dC_M}{d\alpha} + C_A \frac{dY_{cp}}{d\alpha} - C_N \frac{dX_{cp}}{d\alpha}}{\frac{dC_N}{d\alpha} \frac{dC_A C_N}{d\alpha C_A}} , \quad \Delta Y = \frac{C_N}{C_A} \Delta X \qquad (9)$$

The formula sketches the relationship between the CG location (the offset component Y_{cg} and the shift component X_{cg}) and flight requirements, including the trim characteristics (the trimmed α and L/D) and the static pitch stability (the derivative $C_{M,\alpha}$). See [19] for detailed deriving process.

Fig. 11 shows the trimmed α or L/D and the static pitch stability margin distribution in the CG plane. If we have determined the requirements of the trim condition and the static pitch stability, the needed CG position is then exactly located from Fig. 11, which help design the CG of the capsule in the aspect of aerodynamics. Considering the MSL entry capsule, CG is located near the volumetric center (30~50% of the total length) if the capsule mass is relatively uniformly distributed. It

can be seen from the figure that the capsule is statically pitch stable for the small trimmed L/D, and the stability margin is about -0.003/°. The capsule is radially offset for a given degree in the demand of the hypersonic trim condition.

In addition, a small radial bias of CG may cause remarkable flight performance deviation for lifting entry, which should be paid close attention to in the process of aerodynamic design.
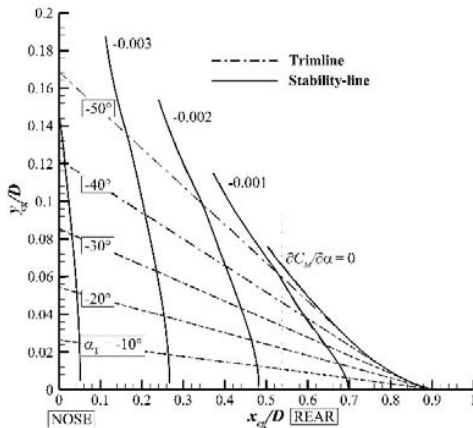

Fig. 11 The trimmed α or L/D and the static pitch stability margin distribution in the CG plane (solid: stability margin isoline, dashed-dot: trimmed α isoline, with the radial direction zoomed in)

IV. CONCLUSIONS

This paper paid great attention to the numerical method for precise simulation of hypersonic Martian flowfield and surface panel method for rapid prediction of aerodynamic coefficients. Detailed flowfield analysis for Mars exploration mission was performed by carrying on a series of fully three-dimensional Navier–Stokes computations. The static aerodynamic performance was then discussed, including the surface pressure, lift and drag coefficient, lift-to-drag ratio with the numerical and engineering method. Calculated results from both methods agree well with each other, and are consistent with the reference data.

Aerodynamic performance analysis shows CG position determines trim characteristics and stability, which can be guidance on aerodynamic design. Specific CG position can be selected so as to fulfill the hypersonic lifting entry. Consequently, proper aerodynamic configuration and cabin equipment layout is needed for CG adjustment to meet the static aerodynamics requirements. This investigation provides researchers with guidelines for the optimization of the design of the Mars entry capsule.

REFERENCES

[1] R.D. Braun, R.M. Manning, Mars exploration entry, descent, and landing challenges, J. Spacecr. Rockets 44 (2) (2007) 310-323.

[2] R. Prakash, P.D. Burkhart, A. Chen, K.A. Comeaux, C.S. Guernsey, D.M. Kipp, D.W. Way, Mars Science Laboratory entry, descent, and landing system overview, in: Proceedings of Aerospace Conference, IEEE, 2008, pp. 1-18.

[3] K.T. Edquist, A.A. Dyakonov, M.J. Wright, C.Y. Tang, Aerothermodynamic environments definition for the Mars Science Laboratory entry capsule, AIAA Pap. 1206 (2007) 8-11.

[4] M.J. Wright, C.Y. Tang, K.T. Edquist, B.R. Hollis, P. Krasa, C.A. Campbell, A review of aerothermal modeling for Mars entry missions, AIAA Pap. 443 (2010) 4-7.

[5] P.A. Gnoffo, K.J. Weilmuenster, R.D. Braun, C.I. Cruz, Effects of sonic line transition on aerothermodynamics of the Mars pathfinder probe, in: Proceedings of AIAA, 1995, 1825-CP.

[6] D.K. Prabhu, D.A. Saunders, On heatshield shapes for Mars entry capsules, in: Proceedings of AIAA, 2002, 1221.

[7] A. Viviani, G. Pezzella, Aerodynamic analysis of a capsule vehicle for a manned exploration mission to Mars, in: Proceedings of the 16th AIAA/DLR/DGLR International Space Planes and Hypersonic Systems and Technologies Conference, AIAA, 2009, 7386.

[8] P.A. Liever, S.D. Habchi, S.I. Burnell, J.S. Lingard, CFD prediction of the Beagle 2 aerodynamic database, in: AIAA (2002) 0683.

[9] E.H. Hirschel, C. Weiland, Selected aerothermodynamic design problems of hypersonic flight vehicles, Springer Press, New York, 2009.

[10] J.D. Anderson, Jr., Hypersonic and high-temperature gas dynamics, AIAA, 2006.

[11] G.J. Brauckmann, J.W. Paulson Jr., K.J. Weilmuenster, Experimental and computational analysis of shuttle orbiter hypersonic trim anomaly, J. Spacecr. Rockets 32 (5) (1995) 758–764.

[12] K.J. Weilmuenster, H.H. Hamilton, A comparison of computed space shuttle orbiter surface pressures with flight measurements, AIAA, 1982, 0937.

[13] R.A. Mitcheltree, P.A. Gnoffo, Wake flow about the Mars pathfinder entry vehicle, J. Spacecr. Rockets 32.5 (1995) 771-776.

[14] K.T. Edquist, P.N. Desai, M. Schoenenberger, Aerodynamics for the Mars Phoenix entry capsule, in: Proceedings of AIAA/AAS Astrodynamics Specialist Conference and Exhibit, AIAA, 2008, 7219.

[15] R.C. Weast, CRC Handbook of Chemistry and Physics, 65th ed. Chemical Rubber Company Press, Cleveland, 1984.

[16] A Fenghour, W.A. Wakeham, V. Vesovic, The viscosity of carbon dioxide, J. Phys. Chem. Ref. Data 27 (1) (1998) 31–44.

[17] M.S. Holden, T.P. Wadhams, G.J. Smolinski, M.G. MacLean, J. Harvey, B.J. Walker, Experimental and numerical studies on hypersonic vehicle performance in the LENS shock and expansion tunnels, AIAA Pap. 125 (2006) 2006.

[18] M. MacLean, M.S. Holden, Catalytic effects on heat transfer measurements for aerothermal studies with CO2, AIAA Pap. 182 (2006) 9-12.

[19] X. Yang, W. Tang, Y. Gui, Y. Du, G. Xiao, L. Liu,Hypersonic static aerodynamics for Mars science laboratory entry capsule, Acta Astronaut. 103 (2014) 168-175.